A New Algorithm for the Quantitation of Myocardial Perfusion SPECT. II: Validation and Diagnostic Yield

Tali Sharir, Guido Germano, Parker B. Waechter, Paul B. Kavanagh, Joseph S. Areeda, Jim Gerlach, Xingping Kang, Howard C. Lewin, and Daniel S. Berman

Departments of Imaging and Medicine and Burns and Allen Research Institute, Cedars-Sinai Medical Center, Los Angeles, California

This study validates a new quantitative perfusion SPECT algorithm for the assessment of myocardial perfusion. The algorithm is not based on slices and provides fully 3-dimensional sampling and analysis independent of assumptions about the geometric shape of the left ventricle. **Methods:** Radiopharmaceutical- and sex-specific normal limits and thresholds for perfusion abnormality in 20 segments of the left ventricle were developed for separate, dual-isotope rest ^{201}Tl–exercise ^{99m}Tc-sestamibi SPECT in 36 patients with <5% before-scanning likelihood of coronary artery disease (CAD) (group 1) and 159 patients with perfusion abnormalities (group 2). These thresholds were validated in 131 patients (group 3) by comparison with expert visual interpretation. Thresholds for automatic segmental scores were developed and validated for groups 2 and 3, respectively. The accuracy of CAD detection was assessed in 94 patients, who underwent coronary angiography (group 4). **Results:** Overall sensitivity for detection of stress and rest segmental perfusion abnormality was 91% and 96%, respectively, for men and 89% and 79%, respectively, for women. Overall specificity for stress and rest was 87% and 90%, respectively, for men and 88% and 90%, respectively, for women. Agreement between automatic and visual scores was good (weighted κ of 0.71 and 0.60 for stress and rest images, respectively). Sensitivity and specificity were 88% for the detection of ≥70% stenosis. For the detection of left anterior descending, left circumflex, and right coronary artery stenosis, sensitivity was 84%, 86%, and 88%, respectively, and specificity was 84%, 88%, and 81%, respectively. **Conclusion:** The new quantitative perfusion SPECT approach is highly sensitive and specific for the detection and localization of CAD, provides accurate automatic scores for the assessment of regional perfusion, and overcomes the low-specificity limitations of previous quantitative algorithms.

Key Words: myocardial perfusion quantitation; dual-isotope imaging; SPECT

J Nucl Med 2000; 41:720–727

Visual interpretation of myocardial SPECT has been shown to provide important diagnostic and prognostic information in various groups of patients with known or suspected coronary artery disease (CAD) (*1–3*). However, substantial intraobserver and interobserver variability in interpretation compromise the reproducibility of the technique and its use in serial assessments of myocardial perfusion (*4*). To overcome these limitations, various approaches for the quantitative analysis of myocardial perfusion SPECT images with ^{201}T1 as well as ^{99m}Tc-sestamibi have been developed and described (*5–9*). Unfortunately, high false-positive rates and the consequent low specificity of these methods in the detection of CAD have limited their use in clinical practice.

We have developed a new approach to quantitative perfusion SPECT that allows accurate 3-dimensional, non–slice-based analysis of relative myocardial perfusion, independent of the size, shape, and orientation of the left ventricle. In addition to a numeric measurement of the extent, severity, and reversibility of perfusion defects, the new approach provides automatic, computer-derived segmental scores, analogous to the semiquantitative 20-segment, 5-point visual scores model, and the option for building customized normal databases. This study was designed, first, to develop sex-specific normal limits and criteria for myocardial perfusion abnormality in patients undergoing dual-isotope rest^{201}T1–exercise ^{99m}Tc-sestamibi SPECT and prospectively validate these criteria; second, to develop and validate criteria for generation of computer-derived segmental scores; and third, to assess the accuracy of this new approach in detecting and localizing CAD.

MATERIALS AND METHODS

Patient Populations

The study population comprised 420 patients who underwent separate, dual-isotope rest ^{201}T1–exercise ^{99m}Tc-sestamibi SPECT. These patients were divided into 4 subgroups.

Normal limits were obtained from 36 patients (18 women, 18 men) (group 1) who, before scanning, had a low likelihood (<5%) of CAD based on sequential bayesian analysis of age, sex, symptom classification, and electrocardiographic response to exercise (*10–12*). Criteria for abnormality were developed using 159 patients (66 women, 93 men) with a wide range of perfusion abnormalities (group 2) and were prospectively validated in 131 patients (73 women, 58 men) referred to our laboratory for

Received Apr. 16, 1999; revision accepted Jul. 30, 1999.

For correspondence or reprints contact: Daniel S. Berman, MD, Department of Imaging, Cedars-Sinai Medical Center, 8700 Beverly Blvd., Rm. A041, Los Angeles, CA 90048.

evaluation of CAD (group 3). The diagnostic yield of the new quantitative algorithm was assessed in 94 patients (15 women, 79 men) who underwent coronary angiography within 90 d of nuclear testing and had no intervening coronary event or revascularization (group 4).

Acquisition Protocol

All patients underwent separate-acquisition dual-isotope myocardial perfusion SPECT as previously described (*13*). Initially, 111–167 MBq (3–4.5 mCi) (dose adjusted to patient weight) ^{201}T1 were injected intravenously at rest, and SPECT was initiated 10 min after injection using a 30% window centered over the 68- to 80-keV energy peak and a 20% window centered over the 167-keV peak. Then, 925–1480 MBq (25–40 mCi) (dose adjusted to patient weight) ^{99m}Tc-sestamibi were injected at the peak of exercise, and SPECT imaging was initiated 15–30 min later using a 15% window centered over the 140-keV photopeak. Images were acquired using a 2-detector 90° camera (Vertex; ADAC Laboratories, Milpitas, CA), a 3-detector camera (Prism; Picker International, Inc., Cleveland Heights, OH), or a 1-detector camera (Orbiter; Siemens Medical Systems, Hoffman Estates, IL) employing 60 or 64 projections over 180° (right anterior oblique 45° to left posterior oblique 45°), low-energy high-resolution collimation, continuous or pseudocontinuous detector rotation, and 35 s (^{201}T1) or 25 s (^{99m}Tc-sestamibi) per projection (*14*). The projection data were reconstructed into tomographic transaxial images using filtered backprojection (*15*). No scatter or attenuation correction was applied. The backprojection used a ramp filter and was preceded by 2-dimensional Butterworth filtering of order 5 and cutoff frequency of 0.25 cycles/pixel for ^{201}T1 or order 2.5 and cutoff frequency of 0.33 cycles/pixel for ^{99m}Tc. Pixel size ranged from 0.53 (Prism) to 0.64 (Vertex) cm. Studies with significant patient motion identified on cine review of the raw scintigraphic data were excluded.

Exercise Protocol

Patients were instructed to discontinue β-blockers and calcium channel antagonists 48 h before testing, and nitrate compounds 6 h before testing, whenever possible. A symptom-limited treadmill exercise test was performed using the Bruce protocol, with continuous monitoring of leads aVF, V_1, and V_5, and 12-lead electrocardiography (ECG) recording of each minute of exercise. Patients received an injection of ^{99m}Tc-sestamibi at peak stress and exercised at the same level for an additional 60 s and then at 1 level lower for 2 min more (*16*). The maximal degree of ST-segment change was measured 80 ms after the J point of the ECG. ECG response was considered diagnostic when horizontal or downsloping ST-segment depression was ≥1 mm or upsloping ST depression was ≥1.5 mm. The response was considered nondiagnostic when ST-T abnormalities were present at baseline ECG. Exercise endpoints were the achievement of ≥85% of maximal predicted heart rate or an ischemic electrocardiographic response. Patients who did not reach 1 of these endpoints were not included in the study. The proportion of patients who achieved at least 85% of maximum heart rate was 100% among those with a low likelihood of CAD and 80% among others. The 20% of patients who did not reach 85% of maximum heart rate had ischemic ECG changes during stress.

Visual Analysis

Stress and rest perfusion SPECT images of patients in groups 2 and 3 were visually scored using a 20-segment model for the left ventricle and a 0–4 scale (0 = normal uptake, 1 = mildly reduced uptake, 2 = moderately reduced uptake, 3 = severely reduced uptake, and 4 = no uptake), as previously described (*13*). Visual scoring was guided by boundaries overlaid on the SPECT slices by quantitative perfusion SPECT. The summed stress score and summed rest score were calculated as the sums of scores of the 20 segments in the stress and rest images, respectively (*13*).

The Quantitation Algorithm

Automatic software analysis started with the identification (segmentation) of the left ventricular myocardium and the extraction of the 3-dimensional endocardial and epicardial surfaces, as described for gated and standard SPECT (*17,18*). Perfusion at each myocardial sampling point was calculated as the average uptake along the count activity profile (endocardial–epicardial segment) normal to the myocardium and passing through that point (*18*). Endocardial and epicardial surfaces were derived even in areas of apparent absence of perfusion using rule-based criteria ensuring the continuity of surface myocardial count profiles (*17*).

Normal Limits and Criteria for Abnormality

Normal limits and abnormality criteria for relative myocardial uptake seen during stress ^{99m}Tc-sestamibi imaging and rest ^{201}T1 imaging were generated separately for men and women. Specifically, normal pixel values (mean ± SD) were calculated from group 1 patients. Abnormality criteria for each of the 20 segments were determined from group 2 by comparing the computer output with the visual scores, using receiver operating characteristic (ROC) analysis. The minimal percentage of abnormal pixels within a segment required to allocate a perfusion defect to that segment was determined. Optimal thresholds for segmental abnormality were prospectively tested in group 3 patients. The global quantitative extent of perfusion defects was calculated by multiplying the number of abnormal segments by 5% (the approximate extent of the myocardium covered by a segment in the 20-segment model).

Automatic Segmental Scores

Relative radiopharmaceutical uptake by each of the 20 myocardial segments was automatically rated using a 5-point scale (0–4) analogous to that used for visual scoring. Thresholds for these automatic computer scores, or CS-20s, were iteratively determined for each visual category so as to maximize agreement between visual and automatic scores for each segment (*18*). The algorithm was developed for group 2 patients—men separately from women—and prospectively validated in group 3 by comparison between computer-derived and visually determined perfusion scores. Rest and stress automatic summed scores were derived from the automatic segmental scores in a manner similar to that for the visual scores.

Assignment of Perfusion Defects to Coronary Territories

A new algorithm, based on hierarchic criteria for the assignment of each of the 20 segments to 1 of the 3 main coronary territories, was developed for localization of perfusion defects. The hierarchic criteria were developed by analyzing a large variety of perfusion abnormality patterns in patients with single and multivessel CAD. The algorithm uses tailored assignment of each of the 20 segments, depending on the pattern of the perfusion defect and the presence or absence of perfusion abnormality in neighboring segments.

Statistical Analysis

Normal limits for the 20 segments were determined as mean ± SD. Criteria for abnormality were determined using ROC analysis

in each of the 20 segments, with the visual score as the gold standard (abnormal when ≥ 2). Optimal sensitivity and specificity were defined as those yielding the minimal value for $(1 - \text{sensitivity})^2 + 0.95 \times (1 - \text{specificity})^2$. Threshold criteria for the automatic CS-20 scores were iteratively obtained by maximizing the agreement (κ) between visual scores and CS-20s. To validate these criteria, weighted κ and SE were calculated for the CS-20s versus visual scores in group 3. Accuracy in the detection and localization of CAD by the quantitative extent of perfusion defects was evaluated by ROC analysis, with coronary angiography as the gold standard. Thresholds for the overall detection of CAD and for detection of CAD in individual territories were defined.

RESULTS

Extent and Localization of Perfusion Defects

The relationship between the extent of perfusion defects determined by quantitative versus visual analysis in group 3 is shown in Figure 1. Both the quantitative and the visual extents of perfusion defects were determined as the proportion of abnormal segments using the respective method. This relationship was linear over a wide range of perfusion abnormality extent in stress and rest images ($r = 0.85$ and 0.87, respectively). Sensitivity and specificity for the detection of perfusion abnormality (visual score ≥ 2) in individual segments are summarized in Table 1. Overall sensitivity in stress and rest images were 91% and 96%, respectively, in men and 89% and 79%, respectively, in women. Specificity in detecting segmental perfusion abnormality was 87% for stress and 90% for rest in men and 88% for stress and 90% for rest in women. Both sensitivity and specificity were higher than 80% in most segments. A relatively too small number of perfusion abnormalities (''positives'') in some segments accounted for the lower sensitivity observed in those segments. The accuracy in the inferior segments (*4,10,16*) in men and in the anterior segments (*1,7,13*) in women was comparable with that of other segments.

Automatic Segmental Scores

A comparison between automatically derived segmental scores and visual segmental scores for stress and rest images in group 3 patients is shown in Tables 2 and 3. A total of

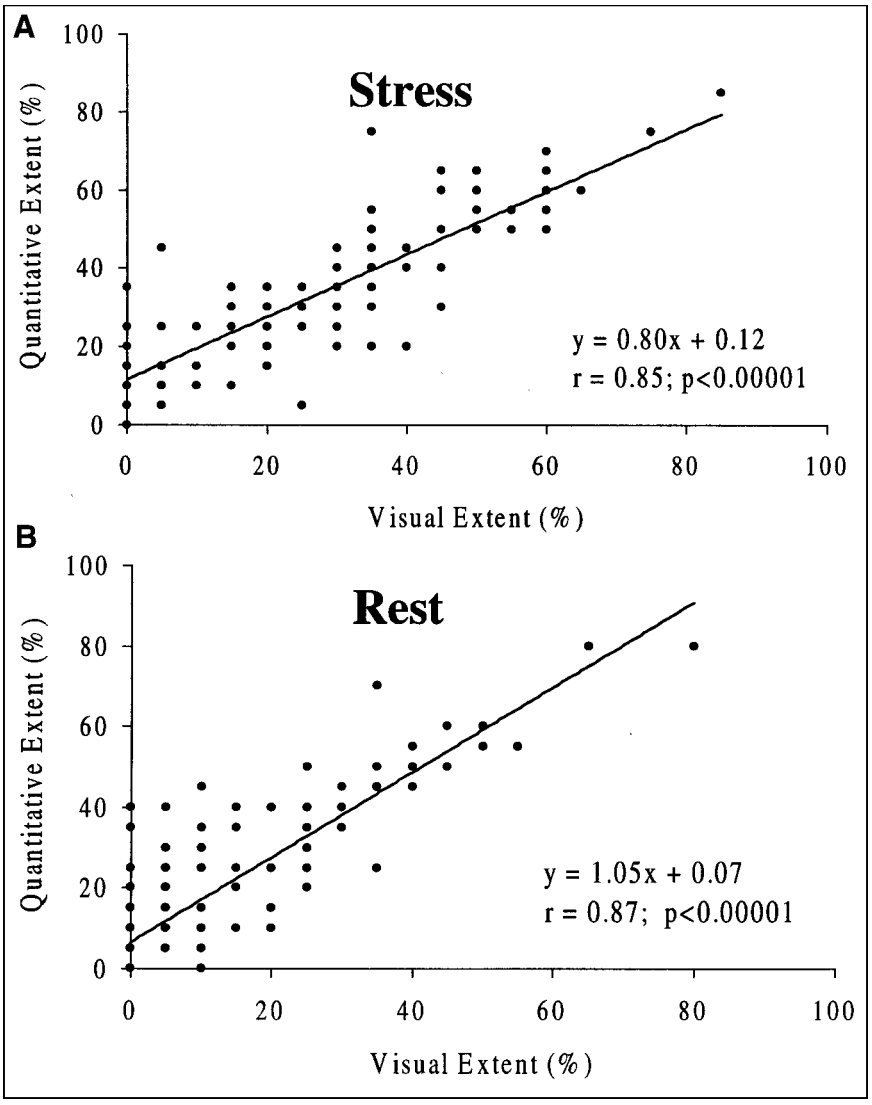

FIGURE 1. Relationship between quantitative and visual extent of perfusion defects (% of left ventricle) in group 3 patients (validation group) at stress (A) and rest (B).

TABLE 1
Sensitivities and Specificities for Detection of Perfusion Abnormality in Individual Segments

Segment no.	Men				Women			
	Stress		Rest		Stress		Rest	
	Sensitivity	Specificity	Sensitivity	Specificity	Sensitivity	Specificity	Sensitivity	Specificity
1	23/31 (94)	23/27 (85)	14/15 (93)	39/43 (91)	26/32 (81)	36/40 (90)	8/12 (67)	59/60 (98)
2	26/27 (96)	30/31 (97)	14/14 (100)	41/44 (93)	17/18 (94)	48/54 (89)	8/9 (89)	58/63 (92)
3	14/17 (82)	36/41 (88)	6/8 (75)	48/50 (96)	9/9 (100)	52/63 (83)	3/4 (75)	66/68 (97)
4	31/38 (82)	19/20 (95)	13/14 (93)	40/44 (91)	38/39 (97)	20/33 (61)	6/10 (60)	53/62 (85)
5	25/26 (96)	20/32 (62)	7/7 (100)	44/51 (86)	29/30 (97)	28/42 (67)	7/7 (100)	55/65 (85)
6	22/22 (100)	30/36 (83)	7/7 (100)	42/51 (82)	15/19 (79)	48/53 (91)	5/7 (71)	61/65 (94)
7	23/26 (88)	30/32 (94)	11/11 (100)	42/47 (89)	14/16 (88)	52/56 (93)	4/5 (80)	64/67 (96)
8	15/15 (100)	31/43 (72)	6/6 (100)	45/52 (87)	10/10 (100)	56/62 (90)	3/3 (100)	58/69 (84)
9	12/12 (100)	40/46 (87)	5/6 (83)	42/52 (81)	5/6 (83)	62/66 (94)	1/1 (100)	68/71 (96)
10	16/21 (76)	36/37 (97)	9/9 (100)	44/49 (90)	21/23 (91)	38/49 (78)	9/9 (100)	46/63 (73)
11	18/19 (95)	31/39 (79)	5/5 (100)	49/53 (92)	19/19 (100)	38/53 (72)	6/8 (75)	58/64 (91)
12	18/18 (100)	33/40 (82)	4/4 (100)	49/54 (91)	9/9 (100)	60/63 (95)	3/3 (100)	66/69 (96)
13	12/13 (92)	40/45 (89)	4/4 (100)	53/54 (98)	3/3 (100)	68/69 (99)	2/2 (100)	54/70 (77)
14	6/7 (86)	47/51 (92)	2/2 (100)	54/56 (96)	2/2 (100)	65/70 (93)	2/2 (100)	63/70 (90)
15	11/13 (85)	37/45 (82)	3/3 (100)	52/55 (95)	5/9 (56)	54/63 (86)	2/4 (50)	64/68 (94)
16	19/20 (95)	33/38 (87)	8/10 (80)	41/48 (85)	10/15 (67)	55/57 (96)	2/5 (40)	65/67 (97)
17	14/15 (93)	40/43 (93)	7/7 (100)	46/51 (90)	10/11 (91)	56/61 (92)	4/6 (67)	57/66 (86)
18	9/10 (90)	48/48 (100)	4/4 (100)	51/54 (94)	4/5 (80)	65/67 (97)	3/4 (75)	63/68 (93)
19	27/28 (96)	29/30 (87)	13/13 (100)	41/45 (91)	33/36 (92)	31/36 (86)	11/13 (85)	51/59 (86)
20	24/28 (86)	26/30 (87)	16/16 (100)	36/42 (86)	25/29 (86)	37/43 (86)	7/7 (100)	55/65 (85)
Overall	371/406 (91)	659/754 (87)	158/165 (96)	899/995 (90)	304/340 (89)	969/1100 (88)	96/121 (79)	1184/1319 (90)

Values in parentheses are percentages.

2600 segments in 130 patients (58 men, 72 women) were analyzed. The observed (exact) agreement, weighted κ, and SE between the 2 scoring methods were 75%, 0.71, and 0.015, respectively, for stress images, and 81%, 0.60, and 0.023, respectively, for rest images. Both values of κ are considered good on the basis of Fleiss's classification (*19*). The correlation between quantitative and visual summed stress scores and summed rest scores is shown in Figure 2. The automatically derived summed stress score and summed rest score correlated linearly to the visual summed stress score ($y = 0.90x + 3.52$, $r = 0.88$, $P < 0.0001$) and summed rest score ($y = 0.97x + 3.2$, $r = 0.86$, $P < 0.0001$), respectively.

Detection of CAD

The results of ROC analysis for detection of overall CAD and individual diseased coronary arteries are shown in Figure 3. A threshold of 3% abnormal pixels in the myocardium provided optimal sensitivity and specificity for the detection of overall CAD. The thresholds that yielded optimal sensitivity and specificity for the detection of stenosis (≥50% or ≥70%) of the left anterior descending artery (LAD), left circumflex artery (LCX), and right coronary artery (RCA) were 3%, 4%, and 2% abnormal pixels within the respective territories.

The overall sensitivity and specificity for the detection of CAD were 83% and 82%, respectively, in detecting ≥50%

TABLE 2
Correlation Between Automatic Scores and Visual Scores at Stress

Visual scores	Automatic scores					
	0	1	2	3	4	Total
0	1472	76	45	5	0	1598
1	54	26	21	0	0	101
2	150	61	302	89	2	604
3	11	2	43	102	31	189
4	2	0	7	46	53	108
Total	1689	165	418	242	86	2600

Agreement = 75%; weighted κ = 0.71; SE = 0.015.

TABLE 3
Correlation Between Automatic Scores and Visual Scores at Rest

Visual scores	Automatic scores					
	0	1	2	3	4	Total
0	1947	65	16	3	1	2032
1	48	23	11	1	0	83
2	149	48	95	40	12	344
3	12	4	16	20	9	61
4	14	4	9	21	32	80
Total	2170	144	147	85	54	2600

Agreement = 81%; weighted κ = 0.60; SE = 0.023.

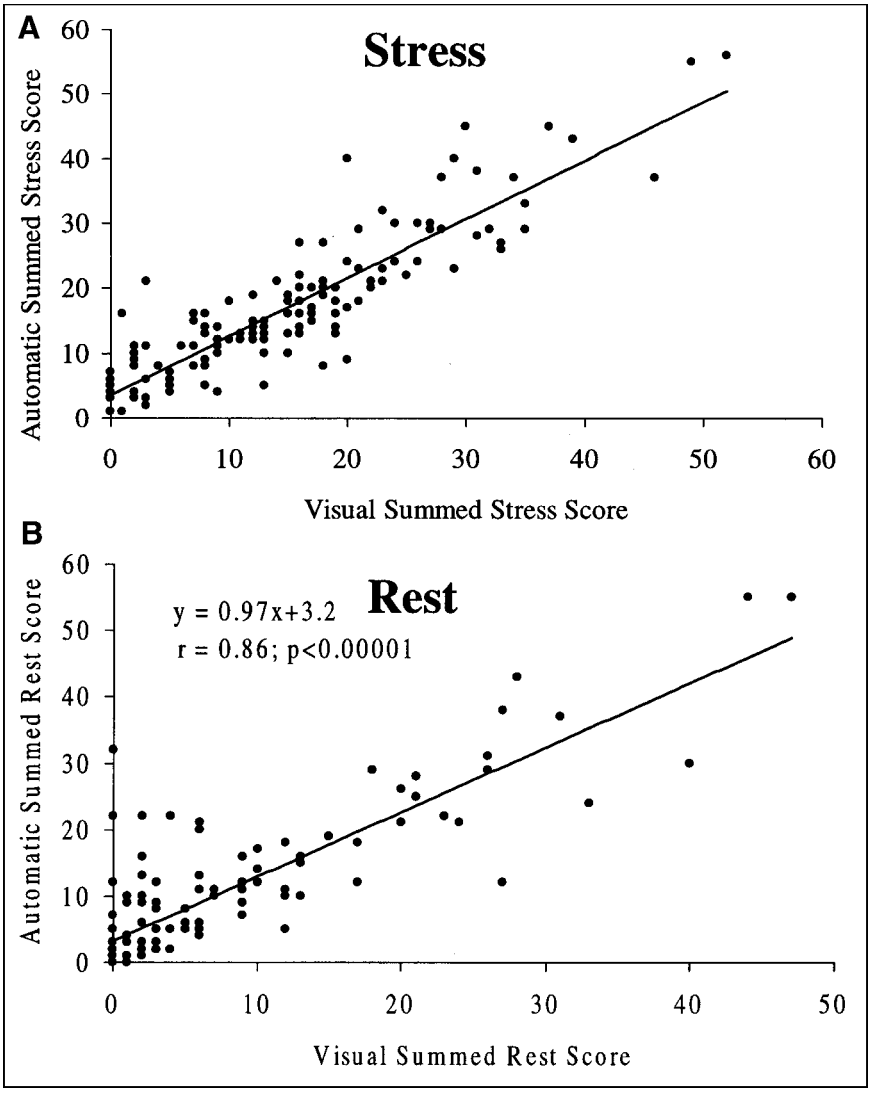

FIGURE 2. Relationship between automatic summed scores and visual summed scores at stress (A) and rest (B) in group 3 patients.

coronary stenosis and 88% (both sensitivity and specificity) in detecting ≥70% coronary stenosis (Fig. 4). The sensitivity and specificity for the identification of individual diseased coronary arteries are shown in Figures 5 and 6. Sensitivity for detection of ≥50% stenosis in the LAD, LCX, and RCA was 75%, 72%, and 73% respectively (Fig. 5). Sensitivities for detection of ≥70% stenosis of the same arteries were higher (84%, 86%, and 88%, respectively). Specificities for the detection of individual artery stenosis were similar (in the range of 80%–90%) for ≥50% and ≥70% diameter narrowing (Fig. 6). Overall sensitivity and specificity were 73% and 85%, respectively, for the detection of any coronary artery with ≥50% narrowing and 86% and 84%, respectively, for any coronary narrowing ≥ 70%.

DISCUSSION

This study validated a new 3-dimensional approach for the quantitation of myocardial perfusion SPECT. Criteria for abnormality were determined for dual-isotope rest ^{201}T1–exercise ^{99m}Tc-sestamibi in training groups for men and women separately and were prospectively validated in a testing group by comparison with expert visual interpretation of the SPECT images. In addition, a method for the automatic generation of quantitative scores was developed and validated by comparison with visual scores. The diagnostic accuracy of the new quantitative method in the detection and localization of CAD was evaluated in patients who underwent coronary angiography.

Comparison with Previous Methods

Most previously described methods of quantitation of myocardial perfusion SPECT use spheric or hybrid spheric–cylindric myocardial sampling techniques, which generate maximal-count circumferential profiles from the short-axis slices (*5–9*). Although the number of these profiles varies with the size of the heart, the number of normal-limits profiles used for patient-profile normalization is fixed. Therefore, those methods are theoretically prone to mapping errors, which may in turn distort the location, size, and severity of perfusion defects as a consequence of normal-

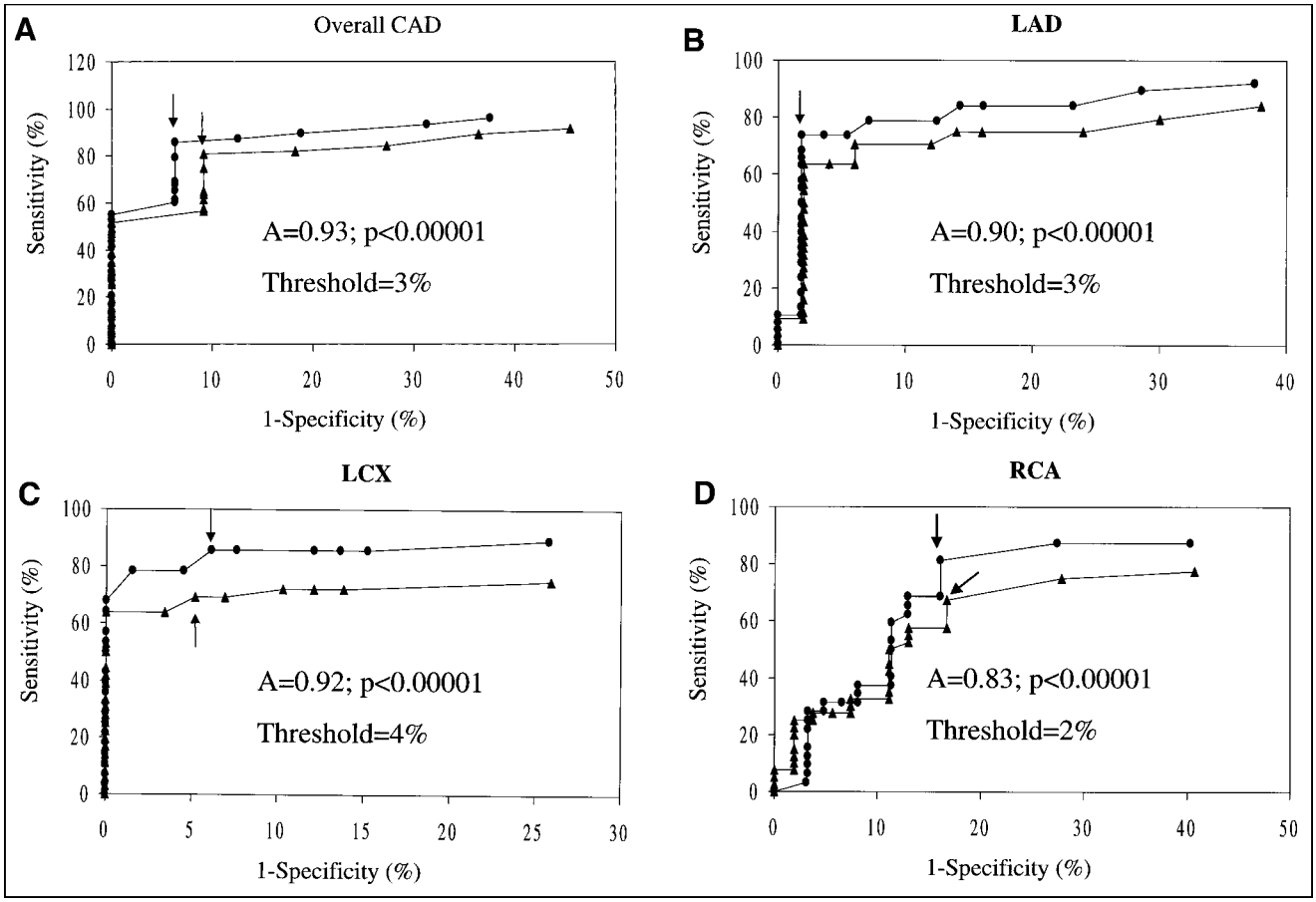

FIGURE 3. Receiver-operator characteristics analysis for detection of overall CAD (A) and individually stenosed coronary arteries (B–D). Arrows indicate sensitivity and 1 − specificity at threshold values. ▲ = ≥50% coronary stenosis; ● = ≥70% coronary stenosis; A = area under curve, derived for ≥70% coronary stenosis.

limits comparison. Indeed, those methods have been reported as having high sensitivity for detection of CAD but low specificity, in the range of 30%–50% (*8,9*). Another method, based on elliptic sampling of radial (long-axis) slices, reported specificity similar (78%) to that we found (*20*).

The new algorithm proposed in this study uses ellipsoid fitting and sampling of the myocardium and generates non–slice-based whole-count profiles encompassing information from the endocardial to the epicardial surfaces rather than just maximal-count circumferential profiles (*18*). Assignment of the sampled data to normal limits does not depend on the size of the patient's myocardium; rather, assignment is based on true 3-dimensional mapping of each sampled data point, consistent with its actual location in the heart. This new method provides intrinsically better matching of patient data with normal limits.

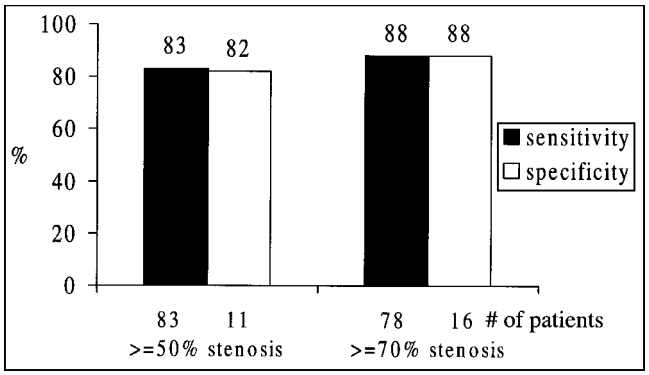

FIGURE 4. Overall sensitivity and specificity for detection of ≥50% and ≥70% coronary stenosis. Number of patients is indicated below each bar.

Normal Limits and Criteria for Abnormality

Because ^{99m}Tc-sestamibi and ^{201}T1 have different physical and biologic characteristics, quantitation of relative uptake of these perfusion agents requires development of agent-specific normal limits and criteria for abnormality (*21,22*). Furthermore, different attenuation patterns in men and women, dominated by diaphragmatic attenuation in men and breast attenuation in women, necessitates assessment of sex-specific thresholds for definition of perfusion abnormality (*8,23*). In this study we developed both agent-specific and sex-specific normal limits and criteria for abnormality. Previous approaches divided the myocardium into 4 major regions (anterior, septal, inferior, and lateral walls) and developed criteria for abnormality for those relatively large

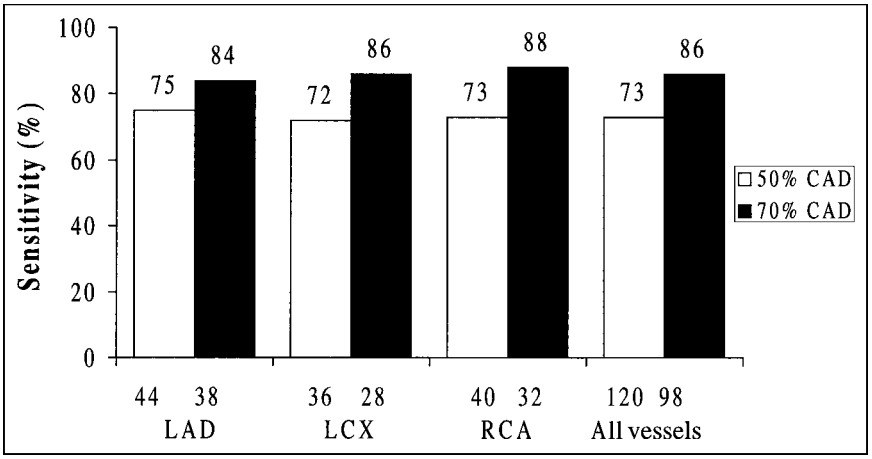

FIGURE 5. Sensitivity for detection of ≥50% and ≥70% stenosis in individual coronary arteries, and overall sensitivity for detection of all individually stenosed coronary arteries. Number of vessels is indicated below each bar.

areas (*8*). This method of defining a single threshold for distal and basal portions of a territory is conceptually subject to inaccuracies, especially in the inferior wall in men and the anterior wall in women, because attenuation within these regions is not homogeneous and often predominates in more basal regions. Our study used the 20-segment model and assessed a separate threshold for each segment. This approach potentially enhances both sensitivity and specificity for the detection of perfusion abnormalities. Indeed, validation of these thresholds yielded high sensitivity and specificity for the detection of perfusion abnormalities at the segmental level.

Automatic Segmental Scores

Summed stress and rest perfusion scores and their difference, based on expert visual interpretation of SPECT images, have been shown to be powerful predictors of outcome in patients with known or suspected CAD (*1–3*). Moreover, the amount of perfusion abnormality at stress, expressed by the summed stress score, has been shown to differentiate between patients at moderate to high risk of both cardiac death and myocardial infarction, who may benefit from revascularization, and patients who are at moderate risk of nonfatal myocardial infarction but low risk of cardiac death, who may benefit from risk factor modification more than from revascularization (*3*). The dependence on expert visual interpretation limits the applicability of these findings. In this study we developed a method for computer-derived segmental scores that provides automatic 5-grade scoring of 20 myocardial segments. The good agreement between quantitative CS-20s and visual scores, and the very good linear correlation between the computer-derived summed stress and rest scores and their homologous visual summed scores, suggest that the CS-20 algorithm may be an extremely effective tool for confirmation of visual reading, useful for diagnosis as well as prognosis assessment.

Accuracy in Detection of Overall and Individual CAD

The threshold of 3% abnormal myocardial pixels for detection of CAD is substantially lower than the 10% threshold value previously reported for ^{99m}Tc-sestamibi quantitation using different techniques (*8,9*). The 3% threshold found with our approach resulted in high sensitivity and specificity for the detection of CAD. Compared with previous studies, although the optimal threshold value was lower the resulting specificity was substantially higher (82%

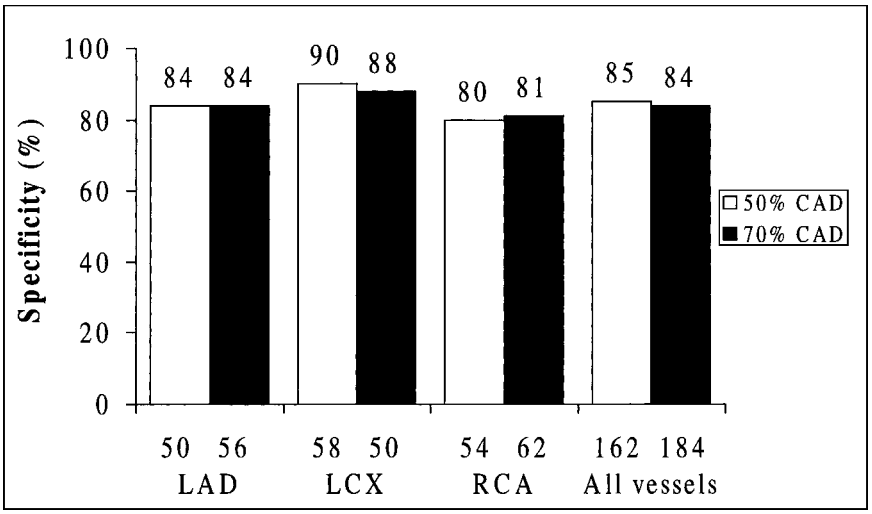

FIGURE 6. Specificity for detection of ≥50% and ≥70% stenosis in individual coronary arteries, and overall specificity for detection of all individually stenosed coronary arteries. Number of vessels is indicated below each bar.

versus 36% for detection of ≥50% CAD and 88% versus 30% for detection of ≥70% CAD) (*9*). These data suggest that even small perfusion abnormalities, in the range of 3%–10% of the left ventricle, may be identified as perfusion defects by the new approach without increasing the false-positive rate.

The thresholds for detection of CAD in the 3 coronary territories on ^{99m}Tc-sestamibi stress images were also considerably lower in this study than in previously reported studies (2%–4% versus 10%–12%). These low thresholds yielded higher sensitivity and specificity for detection of individual diseased coronary arteries than were found with previous methods (*9*). Higher sensitivity was observed in detecting ≥70% stenosis in all 3 coronary arteries, with higher specificity in the LAD and LCX territories. The fixed pattern for grouping segments, used by previous quantitation methods, frequently resulted in false assignment of perfusion defect margins to another territory, reducing specificity in localizing perfusion defects. In contrast, localization of perfusion defects in this study used a rule-based algorithm for segment assignment, which considered the pattern of perfusion abnormality and reduced the frequency of extension, or tailing, of perfusion defects into other territories. This method contributed to low thresholds for abnormality in individual territories and high specificity, without compromising individual vessel sensitivity.

Limitations

No attenuation or scatter correction was used. We believe the accuracy of the approach will likely be greater with an effective attenuation correction algorithm. The patients underwent exercise stress only. Whether the normal limits and thresholds for abnormality defined for exercise stress in this protocol can be applied to pharmacologic stress with vasodilator or inotropic agents remains to be determined.

CONCLUSION

This study developed and validated a new 3-dimensional approach to the automatic quantitation of myocardial perfusion SPECT. Compared with previous methods, this approach provides substantially higher specificity for the detection and localization of CAD, with comparably high sensitivity. In addition, a method for computer-derived segmental scoring of 20 myocardial segments was developed and validated by showing a high correlation to expert-obtained, semiquantitative visual scores.

ACKNOWLEDGMENT

The algorithm described in this work is owned by Cedars-Sinai Medical Center, which receives royalties from its licensing. The authors share a minority portion of those royalties.

REFERENCES

1. Berman DS, Hachamovitch R, Kiat H, et al. Incremental value of prognostic testing in patients with known or suspected ischemic heart disease: a basis for optimal utilization of exercise technetium-99m sestamibi myocardial perfusion single photon emission computed tomography. *J Am Coll Cardiol.* 1995;26:639–647.
2. Hachamovitch R, Berman DS, Kiat H, et al. Exercise myocardial perfusion SPECT in patients without known coronary artery disease: incremental prognostic value and use in risk stratification. *Circulation.* 1996;93:905–914.
3. Hachamovitch R, Berman DS, Shaw LJ, et al. Incremental prognostic value of myocardial perfusion single photon emission computed tomography for the prediction of cardiac death: differential stratification for risk of cardiac death and myocardial infarction. *Circulation.* 1998;97:535–543.
4. Trobaugh GB, Wackers FJ, Sokole EB, DeRouen TA, Ritchie JL, Hamilton GW. Thallium-201 myocardial imaging: an interinstitutional study of observer variability. *J Nucl Med.* 1978;19:359–363.
5. Garcia E, Van Train K, Maddahi J, et al. Quantification of rotational thallium-201 myocardial tomography. *J Nucl Med.* 1985;26:17–26.
6. Van Train KF, Maddahi J, Berman DS, et al. Quantitative analysis of tomographic stress thallium-201 myocardial scintigram: a multicenter trial. *J Nucl Med.* 1990;31:1168–1179.
7. DePasquale EE, Nody AC, DePuey EG, et al. Quantitative rotational thallium-201 tomography for identifying and localizing coronary artery disease. *Circulation.* 1988;77:316–327.
8. Van-Train KF, Areeda J, Garcia EV, et al. Quantitative same-day rest-stress technetium-99m-sestamibi SPECT: definition and validation of stress normal limits and criteria for abnormality. *J Nucl Med.* 1993;34:1494–1502.
9. Van Train KF, Garcia EV, Maddahi J, et al. Multicenter trial validation for quantitative analysis of same-day rest-stress technetium-sestamibi myocardial tomograms. *J Nucl Med.* 1994;35:609–618.
10. Diamond GA, Forrester JS. Analysis of probability as an aid in the clinical diagnosis of coronary artery disease. *N Engl J Med.* 1979;300:1350–1358.
11. Diamond GA, Forrester JS, Hirsch M, et al. Application of conditional probability analysis to the clinical diagnosis of coronary artery disease. *J Clin Invest.* 1980;65:1210–1221.
12. Rozansky A, Diamond GA, Forrester JS, et al. Alternative referent standards for cardiac normality: implications for diagnostic testing. *Ann Intern Med.* 1984;101:164–171.
13. Berman DS, Kiat H, Friedman JD, et al. Separate acquisition rest thallium-201/stress technetium-99m sestamibi dual-isotope myocardial perfusion single-photon emission computed tomography: a clinical validation study. *J Am Coll Cardiol.* 1993;22:1455–1464.
14. Germano G, Van Train K, Kiat H, Berman D. Digital techniques for the acquisition, processing, and analysis of nuclear cardiology images. In: Sandler MP, ed. *Diagnostic Nuclear Medicine*. Baltimore, MD: Williams & Wilkins; 1995:347–386.
15. Germano G, Kavanagh PB, Su HT, et al. Automatic reorientation of three-dimensional, transaxial myocardial perfusion SPECT images. *J Nucl Med.* 1995;36:1107–1114.
16. Berman DS, Kiat H, Germano G, et al. ^{99m}Tc-sestamibi SPECT. In: DePuey GE, Berman DS, Garcia EV, eds. *Cardiac SPECT Imaging*, New York, NY: Raven Press; 1995:123.
17. Germano G, Kiat H, Kavanagh PB, et al. Automatic quantification of ejection fraction from gated myocardial perfusion SPECT. *J Nucl Med.* 1995;36:2138–2147.
18. Germano G, Kavanagh PB, Waechter P, et al. A new algorithm for the quantitation of myocardial perfusion SPECT. 1: technical principles and reproducibility. *J Nucl Med.* 2000;41:712–719.
19. Fleiss JL. *Statistical Methods for Rates and Proportions.* New York, NY: Wiley; 1973.
20. Benoit T, Vivegnis D, Foulon J, Rigo P. Quantitative evaluation of myocardial single-photon emission tomographic imaging: application to the measurement of perfusion defect size and severity. *Eur J Nucl Med.* 1996;23:1603–1612.
21. Leppo JA, Meerdink DA. Comparison of the myocardial uptake of a technetium-labeled isonitrile analogue and thallium. *Circ Res.* 1989;65:632–639.
22. Okada RD, Glover D, Gaffiney T, Williams S. Myocardial kinetics of technetium-99m-hexakis-2-methoxy-2-methylpropyl-isinitrile. *Circulation.* 1988;77:491–498.
23. Eisner RL, Tamas MJ, Cloninger K, et al. Normal SPECT thallium-201 bull's-eye display: gender differences. *J Nucl Med.* 1988;29:1901–1909.